Relativistic Thomas-Fermi calculations of finite nuclei including quantum corrections

D. Von-Eiff[*] and M. K. Weigel[†]

Nuclear Science Division, Mailstop 70A-3307, Lawrence Berkeley Laboratory, University of California, Berkeley, California 94720

(Received 29 June 1992)

Relativistic Thomas-Fermi calculations for finite nuclei including quantum corrections up to second order in $\hbar$, i.e., Wigner-Kirkwood and exchange corrections, have been performed. A linear σ-ω model is used, in case of exchange-corrected calculations extended by π-nucleon and tensor ρ-nucleon contributions. A detailed discussion of the outcome shows that the inclusion of quantum corrections improves the description of the nuclear surface and the classical forbidden region in comparison to the standard relativistic Thomas-Fermi model. Furthermore, special attention is devoted to the investigation of the spin-orbit interaction and the influence of the σ-meson mass on nuclear properties.

PACS number(s): 21.60.−n, 21.10.Dr, 21.10.Ft, 21.10.Gv

I. INTRODUCTION

In recent years the interest in the investigation of nuclear systems has shifted strongly toward a relativistic approach (see, for instance, Refs. [1,2]). The Walecka model (for a review, see Ref. [1]) and its extension by Boguta and Bodmer [3], who added nonlinear contributions through cubic and quartic terms in the scalar field, have been widely and successfully used to describe the ground-state properties of finite systems within the Hartree approximation [1,4,5]. More elaborated and fundamental models, such as the Dirac-Hartree-Fock [6] or Dirac-Brueckner-Hartree-Fock model [7,8], which, moreover, use more sophisticated Lagrangians, have also been investigated.

However, most of these applications are quite involved, because the evaluation of energies and density distributions demands the knowledge of the wave functions of all occupied single-particle states. This can be circumvented by means of semiclassical methods. They allow the study of average nuclear properties in a systematic and transparent way, while the task of calculating the wave functions is avoided, which simplifies the numerical treatment enormously. Within the simplest semiclassical approach, namely, the Thomas-Fermi approximation, the Walecka model has been solved for finite nuclei by several authors [1,9–11].

Semiclassical models including higher-order corrections have been used with great success in *nonrelativistic* nuclear physics (see, for instance, [12,13]). These models are commonly based on the Wigner-Kirkwood (WK) $\hbar$ expansion [14] of the phase-space density, whose lowest order corresponds to the Thomas-Fermi approximation.

Quite recently, several groups have begun to apply semiclassical methods including WK corrections to *relativistic* problems. Because of the matrix structure of the relativistic Hamiltonian, the task of performing the $\hbar$ expansion of the density matrix is much more involved [15–19]. Using this scheme to describe nuclear systems whose potential has to be determined self-consistently, e.g., within the (non)linear σ-ω model, one faces two crucial problems: First, the particle and energy densities including WK corrections up to second order in $\hbar$ are complicated functionals of the meson fields, their first and second derivatives, and the Fermi momenta. To our knowledge, the problem of a *self-consistent* WK approach has not yet been solved in the nuclear context. The second problem is the well-known fact that the WK corrections in coordinate space diverge at the classical turning point. Krivine, Casas, and Martorell [20] pointed out that these are distributions rather than functions in the mathematical sense and can only be used for the computation of expectation values of one-body operators, but not for the determination of r-space densities of any kind to improve the shapes predicted by Thomas-Fermi calculations.

Both of these problems can be overcome by the density-functional formalism, in which the scalar and timelike potentials and their derivatives are eliminated in favor of the corresponding densities and their derivatives. The basic theorem of Hohenberg and Kohn was extended to quantum hadrodynamics (QHD) for the Walecka Lagrangian by Speicher, Dreizler, and Engel [19], thus providing the theoretical foundation of the approach. Numerical investigations within nonlinear σ-ω models were carried out by Centelles *et al.* [21,22].

However, the density-functional approach is not equivalent to the WK approach, because they originate from different arrangements of the $\hbar$ expansion of the energy functional. This is illustrated in Ref. [22] for the case of a given external potential, namely, a relativistic harmonic oscillator: While it can be numerically shown that the WK results up to second order in $\hbar$ are

---

[*]Permanent address: Sektion Physik der Ludwig-Maximilians-Universität München, Theresienstrasse 37/III, W-8000 München 2, Federal Republic of Germany.

[†]Permanent address: Sektion Physik der Ludwig-Maximilians-Universität München, Am Coulombwall 1, W-8046 Garching, Federal Republic of Germany.

equivalent to those obtained by the Strutinsky averaging method, which uses single-particle occupation numbers smoothed by some averaging function to separate the smooth part of the energy from the fluctuating shell corrections [23], the density-functional approach yields different results. It has been shown in the nonrelativistic case that these discrepancies increase within self-consistent calculations [24]. Hence the rearrangement of the $\hbar$ expansion causes some "loss of information," which in turn results in a not so proper estimation of the smooth part of the energy by the density-functional approach. The specific nature of this "loss of information" is one of the questions that we address in this paper.

Like the WK corrections, exchange (Fock) terms are quantal corrections of the order $\hbar$ [17]. Hence, dealing with quantum corrections up to the second order, both kinds of corrections have to be taken into account. Furthermore, exchange corrections allow the study of π-meson and tensor ρ-nucleon contributions to nuclear properties. A semiclassical treatment of such more realistic Lagrangians as used in relativistic Hartree-Fock (RHF) or Brueckner-Hartree-Fock (RBHF) calculations seems to be a meaningful task, since even the RBHF approach can be parametrized in a RHF structure by means of density-dependent coupling constants [25,26].

For all these reasons, we considered it worthwhile to perform semiclassical calculations of finite nuclei including both quantum corrections up to second order in $\hbar$. They are taken into account in a kind of perturbative treatment as outlined in Sec. III. Their impact on average nuclear properties is studied in a systematic way; special attention is devoted to the strength of the spin-orbit interaction, the description of the nuclear surface, and the influence of the σ-meson mass on nuclear properties.

The paper is organized as follows. In Sec. II the expressions of the relativistic Thomas-Fermi approximation (RTFA) within a Walecka model are recalled. The way we incorporated the WK and exchange corrections in our calculations is described in Sec. III. Section IV contains the results and their discussion. Our conclusions are drawn in Sec. V. To complete the paper we give in the Appendix the explicit expressions for the second-order WK corrections to the various densities.

II. RELATIVISTIC THOMAS-FERMI APPROXIMATION

For the sake of completeness, we recall briefly the expressions of the relativistic Thomas-Fermi description of finite nuclei within a Walecka model [1]. The dynamics of the nuclear system are governed by the following Lagrangian, including the electromagnetic field and ρ-meson contributions to take proton-neutron asymmetry effects into account (we use the units $\hbar = c = 1$):

$$\mathcal{L}_1 = \mathcal{L}_N^0 + \sum_{M = \sigma, \omega, \rho, A} [\mathcal{L}_M^0 + \mathcal{L}_{MN}] , \tag{2.1}$$

with the free nucleon and meson Lagrangians

$$\mathcal{L}_N^0(x) = \bar{\psi}(x)(i\gamma_\mu \partial^\mu - M)\psi(x) , \tag{2.2}$$

$$\mathcal{L}_\sigma^0(x) = \tfrac{1}{2}[\partial_\mu \varphi(x)\partial^\mu \varphi(x) - m_\sigma^2 \varphi^2(x)] , \tag{2.3}$$

$$\mathcal{L}_\omega^0(x) = \tfrac{1}{2}m_\omega^2 \omega_\mu(x)\omega^\mu(x) - \tfrac{1}{4}F_{\mu\nu}(x)F^{\mu\nu}(x) , \tag{2.4}$$

$$\mathcal{L}_\rho^0(x) = \tfrac{1}{2}m_\rho^2 \mathbf{b}_\mu(x)\mathbf{b}^\mu(x) - \tfrac{1}{4}\mathbf{G}_{\mu\nu}(x)\mathbf{G}^{\mu\nu}(x) , \tag{2.5}$$

and the free contribution of the electromagnetic field,

$$\mathcal{L}_A^0(x) = -\tfrac{1}{4}A_{\mu\nu}(x)A^{\mu\nu}(x) , \tag{2.6}$$

where the field tensors are given in the usual way:

$$F_{\mu\nu}(x) = \partial_\mu \omega_\nu(x) - \partial_\nu \omega_\mu(x) , \tag{2.7}$$

$$A_{\mu\nu}(x) = \partial_\mu A_\nu(x) - \partial_\nu A_\mu(x) , \tag{2.8}$$

$$\mathbf{G}_{\mu\nu}(x) = \partial_\mu \mathbf{b}_\nu(x) - \partial_\nu \mathbf{b}_\mu(x) . \tag{2.9}$$

The interaction terms $\mathcal{L}_{MN}(x)$ are given by

$$\mathcal{L}_{\sigma N}(x) = g_\sigma \bar{\psi}(x)\varphi(x)\psi(x) , \tag{2.10}$$

$$\mathcal{L}_{\omega N}(x) = -g_\omega \bar{\psi}(x)\gamma^\mu \omega_\mu(x)\psi(x) , \tag{2.11}$$

$$\mathcal{L}_{\rho N}(x) = -g_\rho \bar{\psi}(x)\gamma^\mu \boldsymbol{\tau} \cdot \mathbf{b}_\mu(x)\psi(x) , \tag{2.12}$$

$$\mathcal{L}_{AN}(x) = -e\bar{\psi}(x)\gamma^\mu \frac{1 + \tau_3}{2} A_\mu(x)\psi(x) . \tag{2.13}$$

The Thomas-Fermi expression for the energy density can be derived in a standard way from the Lagrangian. Expanding the nucleon field operators locally into plane waves, while the meson and electromagnetic field operators are replaced by their ground-state expectation values, one gets in the static case

$$e_{TF}(r) = \tfrac{1}{2}\{[\nabla\varphi(r)]^2 + m_\sigma^2 \varphi^2(r)\} - \tfrac{1}{2}\{[\nabla\omega_0(r)]^2 + m_\omega^2 \omega_0^2(r)\} - \tfrac{1}{2}\{[\nabla b_{00}(r)]^2 + m_\rho^2 b_{00}^2(r)\}$$

$$- \tfrac{1}{2}[\nabla A_0(r)]^2 + g_\omega \omega_0(r)b_B(r) + g_b \rho_{00}(r)\rho_3(r) + eA_0(r)\rho_p(r)$$

$$+ \sum_{i = p, n} \frac{1}{8\pi^2}\left[p_F(r)\varepsilon_F^3(r) + p_F^3(r)\varepsilon_F(r) - M^{*4}(r)\ln\frac{p_F(r) + \varepsilon_F(r)}{M^*(r)}\right]_i , \tag{2.14}$$

with the effective mass

$$M^*(r) = M - g_\sigma \varphi(r) , \qquad (2.15)$$

the densities

$$\rho_i(r) = \frac{1}{3\pi^2} p_{F_i}^3(r), \quad i = p, n , \qquad (2.16)$$

$$\rho_B(r) = \rho_p(r) + \rho_n(r) , \qquad (2.17)$$

$$\rho_3(r) = \rho_p(r) - \rho_n(r) , \qquad (2.18)$$

and

$$\varepsilon_{F_i}(r) = [p_{F_i}^2(r) + M^{*2}(r)]^{1/2}, \quad i = p, n . \qquad (2.19)$$

$i = p, n$ denotes the charge state of each nucleon. The assumption of spherical symmetry leaves the timelike components of the vector meson fields, while only the uncharged component of the ρ meson contributes because of charge conservation. We neglect any contribution of antinucleons. In the following the indices of the ω, b, and electromagnetic fields are dropped for simplicity.

The variational principle applied to Eq. (2.14) yields

$$(\Delta - m_\sigma^2)\varphi(r) = -g_\sigma \rho_S(r) , \qquad (2.20)$$

$$(\Delta - m_\omega^2)\omega(r) = -g_\omega \rho_B(r) , \qquad (2.21)$$

$$(\Delta - m_\rho^2)b(r) = -g_\rho \rho_3(r) , \qquad (2.22)$$

$$\Delta A(r) = -e\rho_p(r) , \qquad (2.23)$$

$$\mu_p = g_\omega \omega(r) + g_\rho b(r) + eA(r) + \varepsilon_{F_p}(r) , \qquad (2.24)$$

$$\mu_n = g_\omega \omega(r) - g_\rho b(r) + \varepsilon_{F_n}(r) , \qquad (2.25)$$

with the scalar densities

$$\rho_{S_i}(r) = \frac{2}{(2\pi)^3} \int_0^{p_{F_i}(r)} d^3p \frac{M^*(r)}{[p^2 + M^{*2}(r)]^{1/2}} ,$$
$$i = p, n , \qquad (2.26)$$

$$\rho_S(r) = \rho_{S_p}(r) + \rho_{S_n}(r) . \qquad (2.27)$$

Equations (2.20)–(2.27) constitute a nonlinear system for the nuclear densities, meson, and electromagnetic fields in the RTFA, which has to be solved self-consistently. At each iteration step, the chemical potentials can be adjusted to the right number of protons and neutrons, Z and N, respectively, by

$$\int_V d^3r \, \rho_i(r) = \begin{cases} Z & \text{for } i = p , \\ N & \text{for } i = n . \end{cases} \qquad (2.28)$$

For the kinetic-energy density, one obtains in the RTFA the expression [16]

$$\tau_{\text{TF}}(r) = \sum_{i=p,n} \left\{ \frac{1}{8\pi^2} \left[2p_F(r)\varepsilon_F^3(r) - M^{*2}(r) \left[5 - 4\frac{M}{M^*(r)} \right] p_F(r)\varepsilon_F(r) \right. \right.$$
$$\left. \left. + M^{*4}(r) \left[3 - 4\frac{M}{M^*(r)} \right] \ln\frac{p_F(r) + \varepsilon_F(r)}{M^*(r)} \right] - M\frac{p_F^3(r)}{3\pi^2} \right\}_i . \qquad (2.29)$$

III. QUANTUM CORRECTIONS

In the general Hartree-Fock scheme, the σ meson gives the following contribution to the self-energy in the phase-space representation:

$$\Sigma_\sigma(r, p) = g_\sigma^2 \int_V d^3r' v^{(\sigma)}(r - r')\rho_S(r')$$

$$+ ig_\sigma^2 \int \frac{d^4q}{(2\pi)^4} \frac{1}{(p - q)^2 - m_\sigma^2 + i\eta} G(r, q)$$

$$= \Sigma_\sigma^H(r) + \Sigma_\sigma^F(r, p) . \qquad (3.1)$$

The expressions for the other mesons have a similar structure [17]. $v^{(\sigma)}(r - r')$ represents the static meson propagator (Yukawa potential), while $G(r, q)$ is the Wigner transform of Green's function, which obeys the corresponding Dyson equation. The Wigner transforms of the self-energy and the Dyson equation constitute the relativistic Hartree-Fock approximation in phase space, which is difficult to solve. For that reason we try an approximate solution by utilizing a $\hbar$ expansion. In the next section, we discuss the Wigner-Kirkwood corrections, while Sec. III B deals with the Fock terms.

A. Wigner-Kirkwood corrections

In Ref. [16] we derived the WK corrections to the relativistic phase-space densities and densities up to second order in $\hbar$. The explicit expressions for the second-order terms of the particle, scalar, energy, and kinetic-energy densities of each kind of nucleons "feeling" the action of a scalar and a timelike potential, Σ_S and Σ_0, respectively, are given in the Appendix.

Equations (2.16), (2.26), (2.14), and (2.29) represent the corresponding zeroth-order expressions of the $\hbar$ expansion of Ref. [16], with the energy density e_{TF} depending on the definition of the interaction.

With the dynamics of the system specified by the Lagrangian (2.1), the scalar and timelike parts of the nucleon self-energy are given in each order by

$$\Sigma_S(r) = g_\sigma \varphi(r) , \qquad (3.2)$$

$$\Sigma_{0_p}(r) = g_\omega \omega(r) + g_\rho b(r) + eA(r) , \qquad (3.3)$$

$$\Sigma_{0_n}(r) = g_\omega \omega(r) - g_\rho b(r) , \qquad (3.4)$$

and the general expressions (A5) and (A6) are equivalent

and equal to Eqs. (2.24), (2.25), and (2.15), respectively. The $\hbar$ corrections to the meson and electromagnetic fields are formally determined in each order by a set of equations that are an analog of the Thomas-Fermi equations (2.20)–(2.23) [17]. For the second order, they are explicitly given in the Appendix.

Equations (2.14), (A3) and (2.16), (A1) constitute expressions up to second order in $\hbar$ for the energy and particle density, respectively:

$$e = e_{TF} + \sum_{i=p,n} e_i^{WK} , \qquad (3.5)$$

$$\rho_i = \frac{1}{3\pi^2} p_{F_i}^3 + \rho_i^{WK}, \quad i = p, n . \qquad (3.6)$$

At this point we remind the reader of the two crucial problems we mentioned in the Introduction, namely, the complicated functional dependence of expressions (3.5) and (3.6) on the meson and electromagnetic fields, their first and second derivatives, and the Fermi momenta and second, the divergences of the WK corrections (A1)–(A4) at the classical turning point.

As also mentioned in the Introduction, both of the problems can be overcome by the density-functional formalism [19,21,22], which, on the other hand, "loses information" with respect to the WK approach. To study the impact of the "original" WK corrections, while the simplicity and systematic structure of the semiclassical approach are retained, a kind of *perturbative* treatment seems necessary.

For this purpose we rewrite Eq. (2.28) as

$$\int_V d^3r\, \rho_i(r) = \int_V d^3r \left[\frac{1}{3\pi^2} p_{F_i}^3(r) + \rho_i^{WK}(r) \right]$$

$$= \begin{cases} Z = Z_{TF} + Z_{WK} & \text{for } i = p , \\ N = N_{TF} + N_{WK} & \text{for } i = n , \end{cases} \qquad (3.7)$$

which takes terms of the order $\hbar^2$ into account. To consider the WK corrections within our numerical iteration scheme, we proceeded as follows: After a Thomas-Fermi run of our code (see Sec. II), we used its outcome to calculate the WK corrections to the nucleon densities given by Eq. (A1). Remembering the fact that only WK corrections to expectation values of one-body operators make sense, we integrate those expressions and obtain Z_{WK} and N_{WK} of (3.7). Before starting the next Thomas-Fermi iteration step, the chemical potentials have to be adjusted to the right particle numbers. But now, instead of adjusting them to Z and N, as is done within pure Thomas-Fermi calculations, we use $Z_{TF} = Z - Z_{WK}$ and $N_{TF} = N - N_{WK}$, respectively. This procedure is repeated until convergence is reached. In the final step of calculating the total energy, we include the WK corrections to the energy density and to the meson and electromagnetic fields, as determined by Eqs. (A3) and (A8)–(A11), respectively.

This iteration scheme provides a *perturbative* consideration of the WK corrections to the particle numbers, while their given values Z and N are retained; i.e., comparisons with pure Thomas-Fermi calculations make sense, because one is really looking at the same nucleus.

The perturbative character of the approach ensures that the consideration of the WK corrections is restricted to the order $\hbar^2$; i.e., only zeroth-order quantities are used to calculate Z_{WK} and N_{WK}. In the following we refer to this approximation scheme as RTFA-WK.

B. Exchange corrections

Exchange terms are typical quantum corrections. This can be seen by looking at Eq. (3.1) in a system of units with $\hbar \neq 1$: The Fock terms are at least of the order $\hbar^2$ and hence of the same order as the WK corrections of Eqs. (A1)–(A4) [17]. Therefore, dealing with quantum corrections up to the second order, both kinds of corrections have to be taken into account.

Another motivation to include exchange corrections is the following: As is well known, in the original Walecka (Hartree) model, the incompressibility K of nuclear matter is considerably too large, while the nuclear matter effective mass M^*, which, for fixed saturation density and binding energy determines completely the energy dependence of the optical potential, is too small. A widely and successfully used (see, for instance, Refs. [4,5,9,21,22]) approach to overcome these shortcomings was first proposed by Boguta and Bodmer [3], who introduced two additional free parameters through cubic and quartic terms in the scalar field, which shift K and M^* to more reasonable values compared with the experiment.

On the other hand, nuclear matter calculations within the Hartree-Fock scheme showed [6,27] that to some extend these improvements can also be reached by inclusion of the π meson and an additional tensor coupling term to the ρ-nucleon interaction, but *without* "paying" for it by additional adjustable parameters.

Therefore and because of the arguments given in the Introduction in favor of more sophisticated many-body dynamics, we extend the Lagrangian to the standard Hartree-Fock form (see, for instance, Refs. [6,17,27,28,30])

$$\mathcal{L}_2 = \mathcal{L}_1 + \mathcal{L}_\pi^0 + \mathcal{L}_{\pi N} + \mathcal{L}_{\rho N}^{tensor} . \qquad (3.8)$$

$\mathcal{L}_1$ denotes the original Lagrangian (2.1), while the free π-meson contribution is given by

$$\mathcal{L}_\pi^0(x) = \frac{1}{2}[\partial_\mu \pi(x) \cdot \partial^\mu \pi(x) - m_\pi^2 \pi(x) \cdot \pi(x)] . \qquad (3.9)$$

For the π-nucleon interaction, we use the pseudovector form [6]

$$\mathcal{L}_{\pi N}(x) = -\frac{f_\pi}{m_\pi} \bar{\psi}(x) \gamma_5 \gamma_\mu [\partial^\mu \tau \cdot \pi(x)] \psi(x) , \qquad (3.10)$$

while the tensor part of the ρ-nucleon coupling can be written as

$$\mathcal{L}_{\rho N}^{tensor}(x) = -\frac{f_\rho}{4M} \bar{\psi}(x) \sigma^{\mu\nu} \tau \cdot G_{\mu\nu}(x) \psi(x) , \qquad (3.11)$$

with

$$\sigma^{\mu\nu} = \frac{i}{2}[\gamma^\mu, \gamma^\nu] . \qquad (3.12)$$

The tensor part of the ω-nucleon interaction is negligible [6].

The full self-consistent treatment of the exchange corrections up to second order in $\hbar$ is a rather complicated task [17]. However, it has been shown in Refs. [28,29] that within Hartree-Fock calculations for nuclear matter there are only small deviations when the Fock terms are determined perturbatively with the self-consistently calculated Hartree results as an input, compared with the fully self-consistent procedure. It is also known from nuclear matter Hartree-Fock calculations that Σ_S^F and Σ_0^F, the scalar and timelike components of the exchange part of the nucleon self-energy, respectively, are reasonably independent of momentum and that the corresponding vectorlike component Σ_V^F is a small correction ($<5\%$) to the total nucleon self-energy for the densities of interest in the present study (see, for instance, [6,30]).

For these reasons we proceeded as follows: After a Thomas-Fermi iteration, we used the resulting Fermi momenta and effective mass to calculate $\Sigma_S^F(r,p)$ and $\Sigma_0^F(r,p)$; i.e., the scalar and timelike components of the exchange corrections within a local-density approximation (LDA). To adjust the chemical potentials to the right particle numbers by (2.28), we rewrite Eqs. (2.24) and (2.25) as

$$\mu_p = g_\omega \omega(r) + g_\rho b(r) + e A(r) + \Sigma_{0_p}^F(r)$$
$$+ \{ p_{F_p}^2(r) + [M^*(r) - \Sigma_{S_p}^F(r)]^2 \}^{1/2} , \quad (3.13)$$

$$\mu_n = g_\omega \omega(r) - g_\rho b(r) + \Sigma_{0_n}^F(r)$$
$$+ \{ p_{F_n}^2(r) + [M^*(r) - \Sigma_{S_n}^F(r)]^2 \}^{1/2} ; \quad (3.14)$$

i.e., we treat the scalar and timelike exchange terms, which are calculated within a LDA, like Thomas-Fermi contributions to the nucleon self-energy. As is done in Ref. [30], we take the Fock contributions at the corresponding Fermi momentum. Then the next Thomas-Fermi iteration starts until convergence is reached.

This iteration scheme considers the exchange corrections in a simple way, which allows a systematic study of their impact on the ground-state properties of a given nucleus with mass number $A = Z + N$. In the final step of calculating the total energy, the small corrections of Σ_V^F are also taken into account, calculated with the final Thomas-Fermi outcome in a pure perturbative manner.

Since the explicit expressions for Σ_S^F, Σ_0^F, and Σ_V^F are rather lengthy and given in several publications concerning nuclear matter calculations (see, for instance, Refs. [1,28,31]), we will not repeat them and refer in this respect to the literature.

We denote the approach including the exchange corrections RTFA-EX, while the approximation scheme considering both quantum corrections up to the order $\hbar^2$, WK corrections of Sec. III A, and exchange corrections is referred to as RTFA-QC.

IV. RESULTS AND DISCUSSION

In this section we present the results obtained within the different approximations described in Secs. II and III. For the pure Thomas-Fermi (RTFA) calculations, we used the set of parameters H1 [27], displayed in Table I.

TABLE I. Parameters and nuclear matter properties (energy per particle E/A, Fermi momentum p_F^0, incompressibility K, and effective mass M^*/M at saturation) of the three forces considered in the text. Fixed input parameters are $M = 939$ MeV, $m_\omega = 783$ MeV, $m_\rho = 770$ MeV, and $m_\pi = 138$ MeV; $g_\rho^2/4\pi = 0.55$, $f_\rho/g_\rho = 6.6$, and $f_\pi^2/4\pi = 0.08$. $C_i^2 = g_i^2(M/m_i)^2$, $i = \sigma, \omega$.

	H1	HF1	HF2
m_σ (MeV)	550	550	497
C_σ^2	357.740	288.106	289.474
C_ω^2	274.105	146.656	150.372
E/A (MeV)	−15.75	−15.75	−15.75
p_F^0 (fm^{-1})	1.30	1.30	1.30
K (MeV)	545	394	403
M^*/M	0.541	0.599	0.594

The same parameters are used for RTFA-WK calculations. For the models with exchange corrections, we have chosen the sets HF1 [27] and HF2 [32], which are also given in Table I. The meson masses are fixed to their physical values $m_\omega = 783$ MeV, $m_\rho = 770$ MeV, and $m_\pi = 138$ MeV, while the bare nucleon mass is taken as $M = 939$ MeV. In order not to use too many free parameters, the ρ-nucleon and, in the cases of HF1 and HF2, the tensor ρ- and π-nucleon coupling constants were also fixed to their physical values, namely, $g_\rho^2/4\pi = 0.55$, $f_\rho/g_\rho = 6.6$, and $f_\pi^2/4\pi = 0.08$, known from scattering data [6]. The mass of the σ meson is supposed to represent the exchange of a two-π-resonance and should lie between 400 and 600 MeV. Within Hartree calculations for nuclear matter, m_σ is not an adjustable parameter, because only the ratios of coupling constants to the corresponding meson masses enter the expressions, but by inclusion of Fock terms, the meson masses and hence m_σ occur separately.

Therefore, in the case of H1, there are only two adjustable parameters, the σ- and ω-nucleon coupling constants. Inclusion of exchange corrections (HF1 and HF2) adds the σ-meson mass as free parameter. g_σ and g_ω are chosen to reproduce the empirical saturation point of nuclear matter, $E/A = -15.75$ MeV and $p_F^0 = 1.30$ fm^{-1} ($\rho^0 = 0.1484$ fm^{-3}). In HF1, we retain the value for m_σ from the H1 set (where it has no impact on the nuclear matter results). In HF2, m_σ is adjusted to get the experimental charge rms radius for ^{16}O within our RTFA-QC approach and turns out to be $m_\sigma = 497$ MeV.

As already mentioned earlier, pure Walecka (Hartree) calculations (H1) yield a nuclear matter incompressibility K, which is much too large, while, in view of the energy dependence of the optical potential, the effective mass M^* is too small. As shown in Table I, the consideration of exchange terms shifts K and M^* to not yet perfect but more reasonable values compared with the experimental data. The adjustment of m_σ in HF2 affects the nuclear matter properties only slightly (the variation of K is

smaller than 2.5%), but has significant influence on the results for finite systems, as we will see later.

A. Energies and charge radii

Before discussing the results for the energies and charge rms radii within the different approaches presented in this paper, two remarks have to be made.

First, to obtain expectation values of one-body operators, such as the particle numbers Z and N or the total and kinetic energies E and T_{kin} within the approximations including WK corrections (RTFA-WK and RTFA-QC), one has to evaluate the volume integrals of expressions (A1), (A3), and (A4), respectively. As already mentioned in Sec. I, these expressions are distributions in the mathematical sense with divergences at the classical turning point. Because of this fact, it is not possible to determine r-space densities including WK corrections to improve corresponding Thomas-Fermi predictions. This is a fundamental theoretical restriction of the approaches RTFA-WK and RTFA-QC. On the other hand, the treatment of the divergences while evaluating volume integrals of WK corrections is a purely technical and numerical problem. In the case of a given external potential, Krivine, Casas, and Martorell [20] showed a way to calculate these integrals analytically. This is not possible for a self-consistently determined potential, and thus a numerical "solution" becomes necessary. Performing volume integrals of WK corrections, we used a cutoff at the classical turning point. A possible measure for the quality of this procedure is the reproduction of the particle numbers by Eq. (3.7). The maximum relative error we found is $\sim 0.6\%$ for the neutron number N of ^{16}O within the RTFA-QC approach. In all the other cases, the relative errors for the particle numbers are smaller, for larger nuclei roughly by an order of magnitude. Hence the results including WK corrections can be considered as sufficiently reliable from the numerical point of view.

The second remark concerns center-of-mass corrections to the total energy, $E_{c.m.}$. It was explicitly shown for the nonrelativistic case in Ref. [33] that on a Thomas-Fermi level center-of-mass corrections to the total energy are absent. The inclusion of WK corrections causes center-of-mass corrections. If one treats them in the standard manner, they are overestimated by ~ 30–40% for light and by a factor of ~ 2–3 for heavy nuclei [33]. Because of this reason, we have neglected

them in this study.

We turn now to the discussion of the total energies and charge rms radii calculated within the different approximations described in Secs. II and III. For the characteristic set of spherical nuclei ^{16}O, ^{40}Ca, ^{90}Zr, and ^{208}Pb, the results are displayed in Table II along with the experimental values [6,34–36]. RTFA-EX1, RTFA-QC1 and RTFA-EX2, RTFA-QC2 denote calculations with the set of parameters HF1 and HF2 of Table I, respectively.

For all nuclei under consideration, the inclusion of WK corrections (RTFA-WK) yields considerably stronger bound systems compared with the pure Thomas-Fermi calculations (RTFA). It is the nature of WK corrections containing first and second derivatives of the potentials to improve a Thomas-Fermi approach in the *surface region*, where the RTFA assumption of locally constant meson fields becomes less and less valid. Thus the surface energy is a reasonable candidate when looking for the reason for the stronger binding within the RTFA-WK approach. A proper calculation of the surface energy demands the investigation of a semi-infinite system. In the present paper, we restrict ourselves to a simple estimate. For this purpose we write the semi-empirical mass formula as

$$\frac{E}{A} = -a_V + a_S A^{-1/3} . \qquad (4.1)$$

The volume energy coefficient a_V is given by the energy per nucleon of saturated nuclear matter, namely, $a_V = 15.75$ MeV (see Table I). a_S denotes the surface energy coefficient. We neglect the $A^{-2/3}$ term in the energy expansion (4.1), which is about one order of magnitude smaller than the surface energy. The functional form of the coefficients of the energy expansion up to the order $A^{-2/3}$ follows the droplet-model theory of Myers and Swiatecki [37]. Coulomb and asymmetry energy terms are also omitted in Eq. (4.1), and therefore we recalculated the symmetric systems ^{16}O and ^{40}Ca with the electromagnetic field switched off. Inserting the resulting energies into the left-hand side of expression (4.1), we obtained a decrease of the surface energy coefficient from $a_S \sim 24.5$ MeV within RTFA calculations to $a_S \sim 19.5$ MeV for the RTFA-WK approach, while the experimental value of a_S for symmetric systems is around ~ 20 MeV. Though this procedure gives only a rough estimate of a_S, it allows a qualitative understanding of the

TABLE II. Total energies (in MeV) and charge rms radii (in fm) of ^{16}O, ^{40}Ca, ^{90}Zr, and ^{208}Pb calculated with the different approaches studied in this paper in comparison with the experimental values [6,34–36].

	^{16}O		^{40}Ca		^{90}Zr		^{208}Pb	
	E	r_c	E	r_c	E	r_c	E	r_c
RTFA	-80.85	2.68	-260.28	3.42	-645.98	4.27	-1412.03	5.52
RTFA-WK	-105.51	2.67	-317.36	3.43	-747.85	4.27	-1589.56	5.55
RTFA-EX1	-100.48	2.65	-315.05	3.36	-771.80	4.19	-1671.97	5.40
RTFA-EX2	-79.87	2.75	-273.43	3.43	-703.01	4.24	-1569.36	5.42
RTFA-QC1	-115.12	2.64	-367.04	3.36	-877.90	4.17	-1841.26	5.38
RTFA-QC2	-85.82	2.73	-308.08	3.43	-780.44	4.22	-1711.61	5.40
Expt.	-127.68	2.73	-342.00	3.48	-783.90	4.27	-1636.96	5.42

stronger binding by inclusion of the WK corrections due to a more realistic description of the surface energy.

Comparing RTFA calculations with the RTFA-EX1 approach, where exchange corrections are taken into account, a similar behavior, namely, a stronger binding for all nuclei under consideration, can be observed. Applying the same procedure as described above, we find a decrease of the surface energy coefficient from $a_S \sim 24.5$ MeV for the RTFA approach to $a_S \sim 21$ MeV within RTFA-EX1 calculations. This can be understood in terms of the nuclear matter incompressibility K: Inclusion of exchange corrections along with π-meson and tensor ρ-nucleon contributions while the σ-meson mass m_σ remains fixed causes a significant lower and more realistic value for K (see H1 and HF1 in Table I). A lower incompressibility results in a smaller surface energy, which, in turn, gives a stronger bound system.

Finally, the RTFA-QC1 approach considers WK and exchange corrections. Now both effects—the smaller nuclear matter incompressibility and the improvement of the surface description by consideration of the spatial dependence of the meson fields—operate together, resulting in a further decrease of the surface energy and stronger bindings compared with the RTFA-WK and RTFA-EX1 approaches, where WK and exchange corrections have been considered separately, respectively.

Compared with the experimental values, pure Thomas-Fermi calculations (RTFA) give an underbinding for all nuclei under consideration. Because of the better description of the surface energy, inclusion of WK or exchange corrections shifts the total energies E to more reasonable values (RTFA-WK, RTFA-EX1). Except for the case of ^{16}O, the RTFA-QC1 approach, which considers both quantum corrections, overestimates the binding compared with the experiment. This might be connected with the perturbative character of the approximations as described in Sec. III. Further improvement may be achieved by the consideration of $\hbar$ corrections of higher order.

Looking at the charge rms radii r_c, one realizes that the inclusion of WK corrections hardly affects their values (unsystematic variations of less than 0.5%) compared with pure Thomas-Fermi calculations. The situation is different when exchange corrections are taken into account. Comparing the charge rms radii calculated within the RTFA-EX1 approach with the RTFA results, they are systematically smaller by about 1–2%, consistent with the larger binding energies provided by the inclusion of exchange corrections. A corresponding trend can be observed for the analog "transition" from the RTFA-WK to the RTFA-QC1 approach, which also differ through the consideration of exchange corrections in the latter one. Compared with the experiments [34–36], all the values for r_c within the exchange-corrected approaches RTFA-EX1 and RTFA-QC1 are too small.

As already mentioned earlier, the inclusion of Fock terms into nuclear matter calculations introduces the σ-meson mass m_σ as a third adjustable parameter. We now want to study its impact on the properties of finite systems in a systematic way. In the set of parameters HF2 of Table I, m_σ is adjusted to get the experimental charge radius for ^{16}O within our RTFA-QC approach. The resulting decrease to $m_\sigma = 497$ MeV is not a surprise: The σ-meson contribution represents almost the entire attractive part of the nuclear potential, whose range is therefore determined by m_σ. Thus, for a larger r_c, a smaller m_σ is necessary. As a consequence, for all nuclei under consideration the values for r_c increase within RTFA-EX2 and RTFA-QC2 calculations compared with the RTFA-EX1 and RTFA-QC1 results, respectively, giving a better agreement with the experiments. In addition, the impact of m_σ weakens with increasing mass number A: For ^{16}O, the variations of r_c between HF1 and HF2 calculations are about $\sim 3.5\%$, while for ^{208}Pb those differences go down to $\sim 0.04\%$. This is consistent with the fact that with increasing A the nuclear-matter-like bulk region becomes more and more dominant, and as we mentioned earlier, the impact of m_σ on nuclear matter properties is small (see Table I).

Concerning the binding energies, the systems with larger r_c, calculated with the HF2 set, are less bound than the HF1 nuclei with their smaller charge rms radii. Estimating the surface energy coefficient as described above, the decrease of m_σ from 550 to 497 MeV goes along with an increase of a_S by roughly 4–5 MeV, which fixes it at about the same value as within pure RTFA calculations. Furthermore, the nuclear matter incompressibility rises slightly by 2.3% for the smaller m_σ (see Table I). Thus, for the energy, the effects obtained by the inclusion of exchange corrections in comparison with RTFA are counteracted when m_σ is lowered. As for the charge rms radii, the same trend of a weakening influence of m_σ with increasing mass number A can be observed for the energies. The impact of m_σ on density distributions will be discussed in the following section.

To ascertain the importance of the WK corrections to the energies, it is useful to look at the different contributions in some detail. In Table III we display the WK corrections to the kinetic (T_{kin}^{WK}/A) and potential (E_{pot}^{WK}/A) energies per nucleon along with the remaining

TABLE III. Contributions of the WK corrections to the kinetic (T_{kin}^{WK}/A) and potential (E_{pot}^{WK}/A) energies per nucleon of ^{16}O, ^{40}Ca, ^{90}Zr, and ^{208}Pb within the two approximations RTFA-WK and RTFA-QC1. T_{kin}/A and E_{pot}/A denote the remaining contributions to the total kinetic and potential energies per nucleon. All quantities are in MeV.

RTFA-WK	^{16}O	^{40}Ca	^{90}Zr	^{208}Pb
T_{kin}/A	10.463	9.888	9.860	10.203
T_{kin}^{WK}/A	3.624	3.072	2.443	1.446
E_{pot}/A	−18.050	−18.663	−18.896	−18.133
E_{pot}^{WK}/A	−2.631	−2.232	−1.716	−1.158
RTFA-QC1				
T_{kin}/A	11.656	11.189	10.984	11.214
T_{kin}^{WK}/A	1.930	1.537	1.217	0.814
E_{pot}/A	−19.291	−20.500	−20.802	−19.990
E_{pot}^{WK}/A	−1.489	−1.401	−1.153	−0.890

TABLE IV. Analysis of the total energies of ^{16}O and ^{40}Ca within the different approximations studied in this paper: T_{kin} and E_{Coul} denote the kinetic and Coulomb energies, respectively. E_σ, E_ω, and E_ρ are the Thomas-Fermi contributions to the potential energies coming from the exchange of σ, ω, and ρ mesons, respectively. E_i^{ex}, $i = \sigma,\omega,\rho,\pi,$Coul, denote the corresponding exchange corrections (Fock terms), while E^{WK} is the total WK correction to the energies. The sum of the terms in each column gives the corresponding total energy listed in Table II. All quantities are in MeV.

	^{16}O				^{40}Ca			
	RTFA	RTFA-WK	RTFA-EX1	RTFA-QC1	RTFA	RTFA-WK	RTFA-EX1	RTFA-QC1
T_{kin}	180.94	167.40	187.82	186.49	438.32	395.52	462.63	447.55
E_σ	−2001.68	−2058.49	−1662.15	−1711.60	−5786.36	−5834.05	−4903.21	−4969.13
E_ω	1723.21	1752.20	945.29	963.35	5007.02	5009.59	2803.80	2821.37
E_ρ	0.01	0.02	0.00	0.01	0.06	0.15	0.03	0.06
E_{Coul}	16.88	16.71	17.07	17.21	80.94	78.04	82.48	81.58
E_σ^{ex}			386.86	395.78			1109.13	1113.35
E_ω^{ex}			−190.82	−194.73			−536.23	−536.90
E_ρ^{ex}			67.78	69.96			228.95	230.90
E_π^{ex}			149.75	153.24			442.50	443.89
E_{Coul}^{ex}			−1.95	−1.96			−5.05	−4.97
E^{WK}		15.89		7.05		33.63		5.42

contributions T_{kin}/A and E_{pot}/A within the approaches RTFA-WK and RTFA-QC1 for all nuclei under consideration. T_{kin}^{WK} represents the volume integral of expression (A4), while E_{pot}^{WK} is the difference of the volume integral of Eq. (A3) and T_{kin}^{WK}. We present the energies *per nucleon* to study their dependence on the mass number A. As one expects, the WK corrections decrease with increasing particle number. The values for T_{kin}^{WK}/A and E_{pot}^{WK}/A for ^{208}Pb are 40–60 % smaller than the corresponding ones for ^{16}O, as a result of the greater influence of the surface region in the latter case. A similar, though somewhat smaller, trend can be observed for the WK contributions within the RTFA-WK approach compared with those of RTFA-QC1 calculations: The values in the latter case are significantly smaller, because, as described above, the additionally considered exchange corrections (included in T_{kin}/A and E_{pot}/A) "help" the WK corrections to improve the description of the surface. Finally, in all the cases, the WK corrections mainly "correct" the kinetic energies; their impact on the potential energies is clearly smaller.

The way the total energy is distributed among the various contributions is displayed in Tables IV and V for all nuclei and all approaches under consideration. The upper index "ex" denotes exchange contributions, T_{kin} is, as in Table III, the total kinetic energy without WK corrections, while the total WK corrections are included in E^{WK}. In all cases the dominant contributions are the Thomas-Fermi terms of the σ and ω mesons, E_σ and E_ω, respectively. The corresponding ρ-meson contribution E_ρ is negligible for symmetric nuclei, but has to be considered for ^{208}Pb.

While the nuclear saturation mechanism is almost entirely based on the remarkably balanced cancellation between E_σ and E_ω within the RTFA and RTFA-WK approaches, the situation is modified by the inclusion of exchange corrections. There is a contribution to the attractive part of the nuclear potential by the ω-exchange correction E_ω^{ex} of $\sim 10\%$, while the terms E_σ^{ex}, E_ρ^{ex}, and E_π^{ex} are repulsive, "supporting" E_ω. The π meson, which appears only within the exchange-corrected approaches, contributes 9–10% to the repulsive part of the nuclear potential, while the ρ-meson exchange corrections E_ρ^{ex} are not negligible, independent of the proton-neutron asymmetry of the system. The total sum of each column adds up to the corresponding total energy in Table II.

TABLE V. Same as Table IV for ^{90}Zr and ^{208}Pb.

|	^{90}Zr				^{208}Pb			
	RTFA	RTFA-WK	RTFA-EX1	RTFA-QC1	RTFA	RTFA-WK	RTFA-EX1	RTFA-QC1
T_{kin}	964.20	887.36	1022.46	988.54	2256.92	2122.18	2398.65	2332.52
E_σ	−14070.55	−14157.92	−11993.47	−12086.91	−33876.49	−33610.76	−28926.76	−28965.15
E_ω	12200.23	12202.39	6870.59	6887.64	29342.46	28996.24	16545.90	16519.32
E_ρ	4.58	5.30	4.66	4.67	40.67	43.16	42.09	39.67
E_{Coul}	255.80	249.94	261.32	261.49	824.65	799.31	843.49	851.58
E_σ^{ex}			2688.08	2683.34			6545.70	6503.92
E_ω^{ex}			−1284.52	−1279.74			−3111.80	−3088.02
E_ρ^{ex}			592.53	593.23			1447.94	1446.51
E_π^{ex}			1076.59	1074.19			2563.23	2555.20
E_{Coul}^{ex}			−10.08	−10.06			−20.51	−20.69
E^{WK}		65.45		5.74		59.88		−15.77
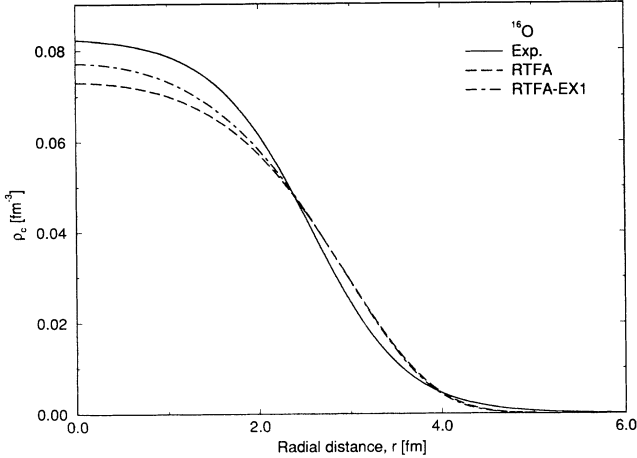
FIG. 1. Charge-density distribution for ^{16}O: Calculated folded values of ρ_c [Eq. (4.2)] within the RTFA and RTFA-EX1 are compared with a three-parameter Fermi fit to the experimental data [34].

B. Densities and spin-orbit interaction

We now turn to the discussion of various nuclear densities. In the previous sections, we have characterized the WK corrections as distributions in the mathematical sense. Therefore plots of r-space densities within the RTFA-WK and RTFA-QC approaches display divergences at the classical turning point. However, we have the interesting possibility to study the impact of exchange corrections by comparing RTFA with RTFA-EX calculations. We may obtain by this comparison essential hints about the role of exchange corrections in a simple manner. One further goal is to study the role of m_σ.

In Figs. 1–4 we present the calculated charge-density distributions ρ_c for all nuclei under consideration within the RTFA and RTFA-EX1 approximations along with three-parameter Fermi fits to the experimental data from Refs. [34–36]. The charge densities are calculated from the proton densities ρ_p (2.16) by
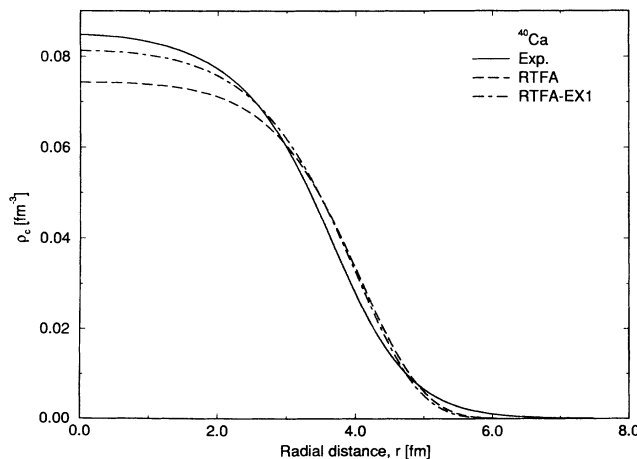
FIG. 2. Same as Fig. 1 for ^{40}Ca.
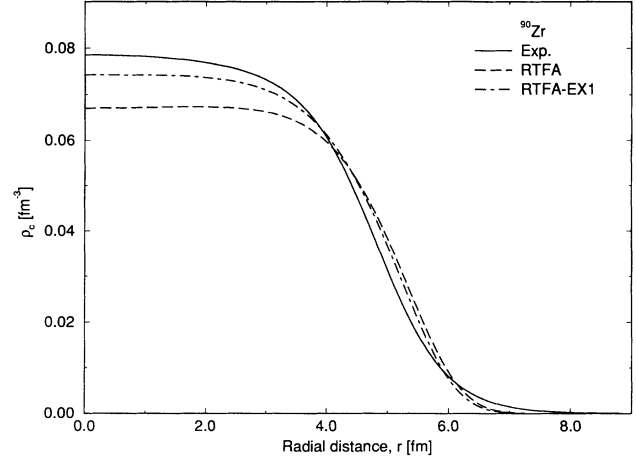
FIG. 3. Same as Fig. 1 for ^{90}Zr. The experimental values are taken from [35].

$$\rho_c(r) = \int d^3r' \frac{1}{(r_0\sqrt{\pi})^3} \exp\left[-\left|\frac{\mathbf{r}-\mathbf{r}'}{r_0}\right|^2\right]\rho_p(r') , \quad (4.2)$$

with $r_0 = \sqrt{2/3}\langle r_p \rangle_{\rm rms}$ and the charge rms radius of the proton taken as $\langle r_p \rangle_{\rm rms} = 0.8$ fm [6]. Compared with the experiments, the calculated RTFA densities are systematically too small in the bulk. Furthermore, the experimental surface behavior (steepness) is not reproduced. Additionally, as expected, the quantal tails cannot be described correctly in a Thomas-Fermi treatment.

By inclusion of exchange corrections through the RTFA-EX1 approach, the bulk value of the charge density increases considerably in all cases; for ^{208}Pb, it is in good agreement with the experiment. This corresponds to the higher binding energies for RTFA-EX1 nuclei, as discussed in the previous section (see Table II). Furthermore, the smaller sizes provided by RTFA-EX1 calculations compared with RTFA are reflected in the density
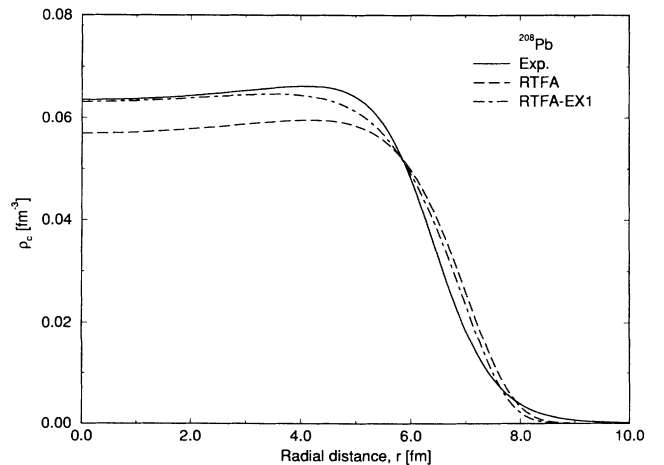

FIG. 4. Same as Fig. 1 for ^{208}Pb. The experimental values are taken from [36].

shapes: For ^{16}O, inclusion of exchange terms reduces r_c by 1.1%. This relative reduction increases with A and is twice as large for ^{208}Pb (see Table II). This A-dependent effect is clearly visible comparing the long-dashed and dot-dashed lines of Figs. 1–4. Because the exchange terms are treated like Thomas-Fermi contributions to the nuclear potential—i.e. they are averaged in the same way (see Sec. III B)—one cannot expect any improvement in the quantal tails and, of course, no shell effects are obtainable in both treatments.

As mentioned in the previous section, changes in m_σ influence mainly small systems, while their impact is weakened for large nuclear-matter-like nuclei. To study the m_σ dependence of particle densities, we therefore look at the baryon densities ρ_B [see Eq. (2.17)] of the small systems ^{16}O and ^{40}Ca. This is done in Figs. 5 and 6, where we have plotted the RTFA, RTFA-EX1, and RTFA-EX2 results. As for the charge densities of Figs. 1–4, the bulk values of ρ_B are higher within the RTFA-EX1 approximation compared with the RTFA. The counteracting effect of a decreasing m_σ we discussed in the previous section and which leads to weaker bindings in RTFA-EX2 compared with RTFA-EX1 (see Table II) yields, in turn, reduced corresponding bulk values of ρ_B. The diffuseness of the RTFA-EX2 densities are larger than the RTFA-EX1 ones. We observed similar trends for the charge densities, indicating that the higher values for the charge rms radii in RTFA-EX2 (see Table II) are obtained by the longer tails of the charge densities rather than by an actual increase of the systems sizes. Confirming our previous statement concerning the dependence of the impact of m_σ on the mass number A, the differences between the RTFA-EX1 and RTFA-EX2 baryon densities are smaller for ^{40}Ca than for ^{16}O. We found that for ^{90}Zr and ^{208}Pb this trend continues.

We now turn to the discussion of kinetic-energy densities. In Fig. 7 we present the proton kinetic-energy densities τ_p for our set of spherical nuclei within the RTFA
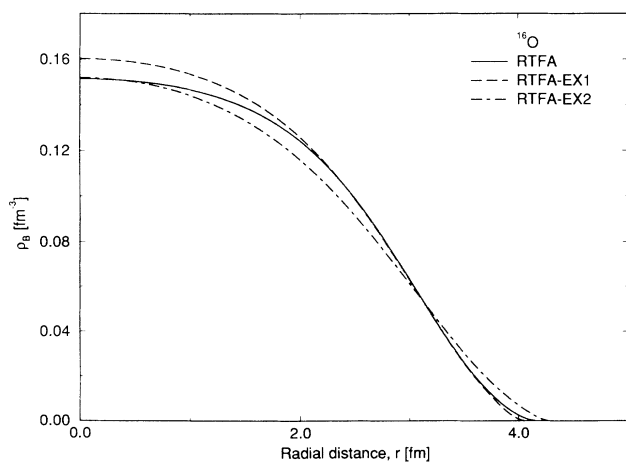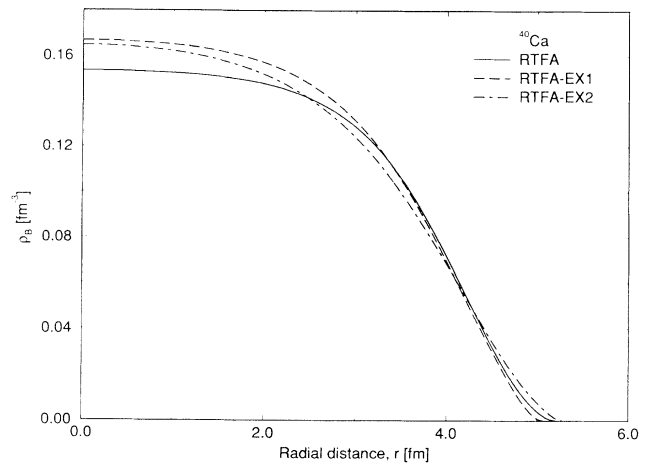

FIG. 6. Same as Fig. 5 for ^{40}Ca.

(solid lines), RTFA-EX1 (long-dashed lines), and RTFA-EX2 (dot-dashed lines) approximations. As for the charge and baryon densities of Figs. 1–6, the values in the bulk are considerably higher when exchange terms are included. Comparing the RTFA-EX1 with the RTFA-EX2 results, the impact of m_σ in the bulk region is not as systematic as discussed above. However, similar to Figs. 5 and 6, a more diffuse falloff can be observed for the RTFA-EX2 interaction compared with RTFA-EX1. The peaks in the surface regions, even for the small nuclei where no central depression caused by the electromagnetic field occurs, reflect the dependence of the kinetic-energy density on the effective mass [see Eq. (2.29) for the RTFA], which approaches the bare nucleon mass at large radial distances.

At all radial distances, τ_p is positive. This is what one expects for the semiclassical RTFA model as well as for the RTFA-EX approaches, where exchange terms are treated as Thomas-Fermi contributions to the nuclear potential (see Sec. III B). These approximations are principally not able to describe the physics of the classically forbidden region, where the quantal tails of the particles' wave functions have negative kinetic energies, resulting in a negative kinetic-energy density in the outer surface region. However, improvement of this deficiency of standard Thomas-Fermi methods is one of the reasons for the consideration of WK corrections. Hence we plotted in Fig. 8 the Thomas-Fermi contribution τ_p^{TF} [see Eq. (2.29)] and the total proton kinetic-energy density $\tau_p = \tau_p^{TF} + \tau_p^{WK}$ of ^{208}Pb within our RTFA-WK approach [τ_p^{WK} is given by Eq. (A4)]. Of course, this is "illegitimate" in view of the WK corrections being distributions in the mathematical sense (see Sec. III A), and the question concerning the physical nature of such a plot, and especially of the divergences, finally remains open to us (in this context, see also Ref. [38]). However, considering the fact that the volume integral of τ_p is a reasonable physical quantity, it might be of interest that, while τ_p^{TF} stays positive at all radial distances as expected, the inclusion of WK corrections yields a negative kinetic-energy density in the surface re-

FIG. 5. Baryon density for ^{16}O: Calculated point (unfolded) values of ρ_B [Eq. (2.17)] within the RTFA, RTFA-EX1, and RTFA-EX2 approaches.
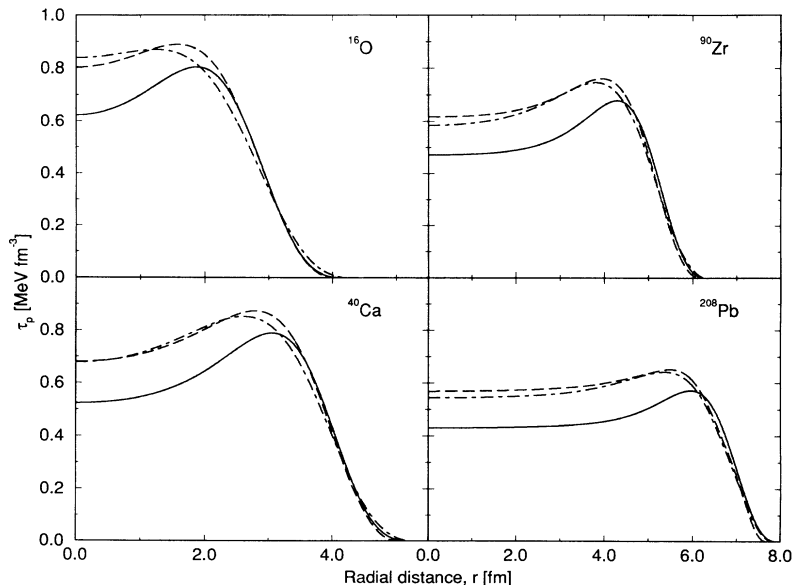
FIG. 7. Proton kinetic-energy densities for all nuclei under consideration obtained in the RTFA (solid lines), RTFA-EX1 (long-dashed lines), and RTFA-EX2 (dot-dashed lines) approximations.

gion before it diverges at the classical turning point. Referring to the vague "loss of information" along with the reordering of the $\hbar$ expansion when going from the WK approach to the density-functional formalism (see Sec. I), this negative kinetic-energy density might be a candidate: Looking at Fig. 5 of Ref. [21], the density-functional formalism seems not to be able to provide negative values for τ_p at large radial distances (in a recent paper, Swiatecki [39] studied an improved nonrelativistic Thomas-Fermi method, in which the standard expression for the kinetic-energy density is modified so that it becomes negative in the outer surface region).

Finally, we turn to the discussion of the *spin-orbit interaction*. It is automatically included in the single-particle Dirac equation and can be identified by means of
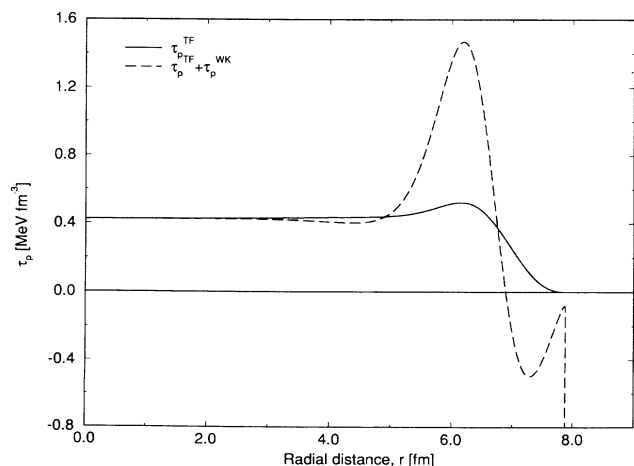
FIG. 8. RTFA contribution (solid line) and total (long-dashed line) proton kinetic-energy "density" of ^{208}Pb within the RTFA-WK approach.

a Foldy-Wouthuysen reduction. For a nucleon "feeling" the action of a scalar and a timelike potential, Σ_S and Σ_0, respectively, one obtains an effective single-particle spin-orbit interaction of the form [1,40]

$$V_{\text{s.o.}}(r) = \frac{1}{2M^2 r}\left[\frac{d\Sigma_0(r)}{dr} + \frac{d\Sigma_S(r)}{dr}\right]\mathbf{S}\cdot\mathbf{L}$$

$$\equiv -\alpha(r)\mathbf{S}\cdot\mathbf{L} . \tag{4.3}$$

We calculated the quantity α for a proton in all nuclei under consideration. Within the RTFA, Σ_S and Σ_0 are given by Eqs. (3.2) and (3.3), respectively. For RTFA-EX calculations, we used, in accordance with Eq. (3.13),

$$\Sigma_S(r) = g_\sigma\varphi(r) + \Sigma_{S_p}^F(r) , \tag{4.4}$$

$$\Sigma_0(r) = g_\omega\omega(r) + g_\rho b(r) + eA(r) + \Sigma_{0_p}^F(r) , \tag{4.5}$$

with the Fock contributions evaluated at the corresponding Fermi momentum. The results are presented in Fig. 9. While Σ_S and Σ_0 are adding up in the spin-orbit interaction of Eq. (4.3), we know that they tend to cancel in the binding energy. Therefore we also plotted the differences of the scalar and timelike components of the RTFA proton self-energies, $\Sigma_S - \Sigma_0$, in Fig. 9. These differences become negative for large radial distances because of the long-range Coulomb field, which is included in Σ_0.

The interesting parts are the peaks of α in the surface regions. It can be observed that the inclusion of exchange corrections (RTFA compared with RTFA-EX1 results) reduces the maximum value of α by roughly 9–12 %, while the lower m_σ (RTFA-EX1 compared with RTFA-EX2) causes an additional decrease of α_{max} of about the same magnitude. This latter effect is consistent with the larger diffuseness of RTFA-EX2 densities we discussed above.

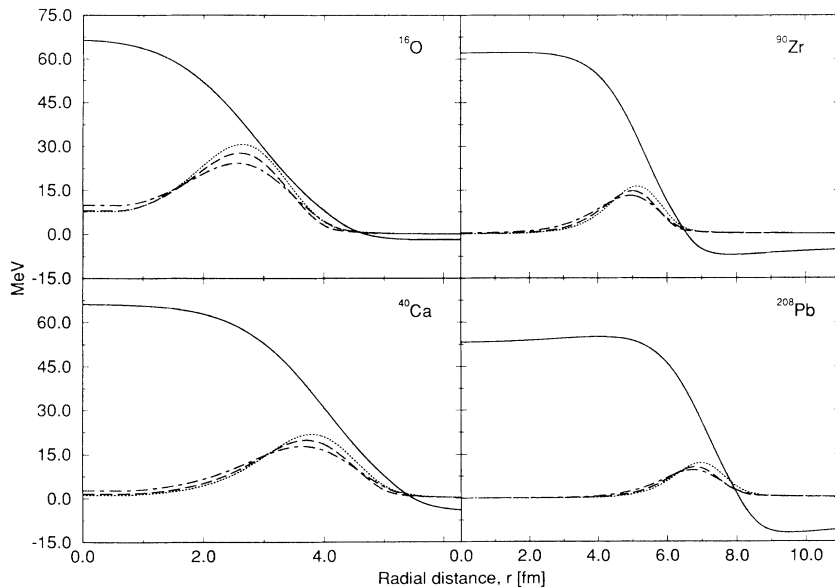Furthermore, α_{max} depends strongly on the mass num-

FIG. 9. Radial distribution of the quantity $10\alpha(r)$ for a proton in all nuclei under consideration obtained in the RTFA (dotted lines), RTFA-EX1 (long-dashed lines), and RTFA-EX2 (dot-dashed lines) approximations along with the difference of the scalar and timelike components $(\Sigma_S - \Sigma_0)$ of the RTFA proton self-energy (solid lines).

ber A. Within the RTFA we found $\alpha_{max} = 3.08$ MeV for ^{16}O, but $\alpha_{max} = 1.19$ MeV for ^{208}Pb. This is clear in view of the larger radial distances involved for larger systems [see expression (4.3)] and means, in turn, that the strength of the spin-orbit splitting decreases with increasing orbital angular momentum. This trend agrees with experimental data (see Ref. [41]). Finally, we compare our results for α_{max} in ^{40}Ca with the experimental value of the spin-orbit splitting for the odd proton in ^{41}Sc: within RTFA, RTFA-EX1, and RTFA-EX2 calculations, we obtained $\alpha_{max} = 2.19$, 1.99, and 1.78 MeV, respectively, while the experiment yields $\alpha = 1.80$ MeV [10]. Hence our exchange-corrected model is in rather close agreement with the empirical data.

V. CONCLUDING REMARKS

In the present paper, we have carried out relativistic Thomas-Fermi calculations including quantum corrections for a set of spherical nuclei. There are two kinds of quantum corrections up to the second order in $\hbar$, which we incorporated perturbatively in our code, while the numbers of protons and neutrons are held fixed. First are the WK corrections, which are supposed to improve the expectation values of one-body operators compared with pure Thomas-Fermi calculations. In this case we used a linear σ-ω model which reproduces the nuclear matter saturation point, but yields a considerably too large nuclear matter incompressibility. The latter point causes a surface energy, which is too high within Thomas-Fermi calculations. Inclusion of WK corrections significantly reduces the difference between the RTFA and experimental value of the surface energy coefficient, resulting in more realistic binding energies. This improvement within the RTFA-WK approximation is achieved by a better description of the nuclear surface through consideration of the spatial dependence of the meson and electromagnetic fields and the possibility of a negative

kinetic-energy density in the surface region which characterizes the physics of the classical forbidden region. The impact of the WK corrections decreases with increasing mass number.

The second kind of quantum corrections of the order $\hbar^2$ are exchange corrections. Here we also considered π-meson and tensor ρ-nucleon contributions. This shifts the nuclear matter incompressibility to more reasonable values. In turn, we found the nuclear surface energy lowered by the exchange corrections by $\sim 14\%$, which yields stronger bindings and smaller charge rms radii compared with the RTFA approach. As a consequence, the bulk values of the charge, particle, and kinetic-energy densities are systematically higher within RTFA-EX calculations.

Within nuclear matter Hartree-Fock calculations, m_σ constitutes an adjustable parameter. We calculated a set of parameters with m_σ adjusted to get the experimental charge rms radius of ^{16}O and studied its influence on properties of nuclear matter and finite nuclei. While m_σ affects nuclear matter properties only slightly, it has significant influence on those of finite systems. With the σ-meson contribution representing almost the entire attractive part of the nuclear potential, m_σ determines its range. Hence we found that a lower m_σ yields larger rms radii, weaker bindings, and lower bulk values of the various densities. The larger rms radii go along with a more diffuse falloff in the surface regions of the densities we investigated. The impact of m_σ weakens with increasing mass number according to the nuclear matter limit, where its influence is small.

Finally, we calculated the spin-orbit interaction. We found that its strength decreases with both the inclusion of exchange corrections and decreasing m_σ. In agreement with experimental data, a strong dependence of the spin-orbit splitting on the mass number can be observed, namely, smaller values with increasing A. The maximum

value of the spin-orbit splitting we found within RTFA-EX calculations for a proton in ^{40}Ca is in good agreement with the experiment.

In summary, by including quantum corrections in the described approximate manner, our approach constitutes a simple and transparent model to study their impact on the properties of finite systems in a systematic way for nontrivial Lagrangians along with a tractable numerical effort in comparison with lengthy wave-function calculations.

ACKNOWLEDGMENTS

APPENDIX

In this appendix we give the explicit expressions for the second-order WK corrections to the particle, scalar, energy, and kinetic-energy densities of *each kind of nucleon* "feeling" the action of a scalar and a timelike potential Σ_S and Σ_0, respectively (see Ref. [16]):

$$\rho^{\mathrm{WK}}(r) = \frac{1}{24\pi^2}\left[\frac{1}{p_F}(3-x_F^2)(\nabla\Sigma_0)^2 - \left[2x_F+4\ln\frac{p_F+\varepsilon_F}{M^*}\right]\Delta\Sigma_0 + 2\frac{x_F}{M^*}(3-x_F^2)\nabla\Sigma_0\cdot\nabla M^* \right.$$
$$\left. + \frac{1}{p_F}(2-x_F^2)(\nabla M^*)^2 + 2\frac{p_F}{M^*}(1-x_F^2)\Delta M^* \right], \tag{A1}$$

$$\rho_S^{\mathrm{WK}}(r) = -\frac{1}{24\pi^2}\left[\frac{x_F}{M^*}(1+x_F^2)(\nabla\Sigma_0)^2 + 2\frac{M^*}{p_F}\Delta\Sigma_0 + \frac{2}{p_F}(2+x_F^2)\nabla\Sigma_0\cdot\nabla M^* + \frac{x_F}{M^*}(2+x_F^2)(\nabla M^*)^2 \right.$$
$$\left. + \left[2x_F-6\ln\frac{p_F+\varepsilon_F}{M^*}\right]\Delta M^* \right], \tag{A2}$$

$$e^{\mathrm{WK}}(r) = \frac{1}{24\pi^2}\left[\left[x_F(2-x_F^2)-2\ln\frac{p_F+\varepsilon_F}{M^*}\right](\nabla\Sigma_0)^2 - 2p_F(1+x_F^2)\Delta\Sigma_0 + 2\frac{M^*}{p_F}(1-x_F^2)\nabla\Sigma_0\cdot\nabla M^* \right.$$
$$\left. + \left[x_F(1-x_F^2)-\ln\frac{p_F+\varepsilon_F}{M^*}\right](\nabla M^*)^2 - 2M^*\left[x_F-\ln\frac{p_F+\varepsilon_F}{M^*}\right]\Delta M^* \right]$$
$$+ \left[1-\frac{\lambda}{2}\right]\Sigma_0\rho^{\mathrm{WK}}(r) + \frac{\lambda}{2}\Sigma_S\rho_S^{\mathrm{WK}}(r), \tag{A3}$$

$$\tau^{\mathrm{WK}}(r) = \frac{1}{24\pi^2}\left\{\left[\left[3-(1+x_F^2)\frac{M}{M^*}\right]x_F-(3-x_F^2)\frac{M}{p_F}-2\ln\frac{p_F+\varepsilon_F}{M^*}\right](\nabla\Sigma_0)^2 \right.$$
$$+ 2M\left[x_F-\frac{p_F}{M}\left[2-(1-x_F^2)\frac{M}{M^*}\right]+2\ln\frac{p_F+\varepsilon_F}{M^*}\right]\Delta\Sigma_0$$
$$- \left[\frac{2M}{p_F}(2+x_F^2)+2x_F\frac{M}{M^*}(3-x_F^2)+6\frac{p_F}{M^*}(1-x_F^2)\right]\nabla\Sigma_0\cdot\nabla M^*$$
$$- \left[\frac{M}{p_F}(2-x_F^2)-\left[3-2\frac{M}{M^*}\right]x_F+\frac{M}{M^*}x_F^3+\ln\frac{p_F+\varepsilon_F}{M^*}\right](\nabla M^*)^2$$
$$\left. -2M\left[x_F+\frac{p_F}{M^*}(1-x_F^2)-\left[3-2\frac{M^*}{M}\right]\ln\frac{p_F+\varepsilon_F}{M^*}\right]\Delta M^* \right\}, \tag{A4}$$

with ε_F given by (2.19) and the definitions

$$p_F(r):=\{[\mu-\Sigma_0(r)]^2-M^{*2}(r)\}^{1/2}, \tag{A5}$$

$$M^*(r):=M-\Sigma_S(r), \tag{A6}$$

and

$$x_F(r):=\frac{\varepsilon_F(r)}{p_F(r)}. \tag{A7}$$

In Eq. (A3), $\lambda=0$ corresponds to a purely external potential, while $\lambda=1$ describes the case of a self-consistent two-particle interaction.

For the Lagrangian (2.1), the decomposition of Σ_S and Σ_0 is given in each order of $\hbar$ by Eqs. (3.2)–(3.4). The second-order corrections to the meson and electromagnetic fields are determined by [17]

$$(\Delta - m_\sigma^2)\varphi^{WK}(r) = -g_\sigma[\rho_{S_p}^{WK}(r) + \rho_{S_n}^{WK}(r)] , \tag{A8}$$

$$(\Delta - m_\omega^2)\omega^{WK}(r) = -g_\omega[\rho_p^{WK}(r) + \rho_n^{WK}(r)] , \tag{A9}$$

$$(\Delta - m_\rho^2)b^{WK}(r) = -g_\rho[\rho_p^{WK}(r) - \rho_n^{WK}(r)] , \tag{A10}$$

$$\Delta A^{WK}(r) = -e\rho_p^{WK}(r) . \tag{A11}$$

[1] B. D. Serot and J. D. Walecka, in *Advances in Nuclear Physics*, edited by J. W. Negele and E. Vogt (Plenum, New York, 1986), Vol. 16, and references therein.

[2] L. S. Celenza and C. M. Shakin, in *Relativistic Nuclear Physics, Lecture Notes in Physics*, Vol. 2 (World Scientific, Singapore, 1986), and references therein.

[3] J. Boguta and A. R. Bodmer, Nucl. Phys. **A292**, 413 (1977).

[4] Y. K. Gambhir, P. Ring, and A. Thimet, Ann. Phys. (N.Y.) **198**, 132 (1990).

[5] P.-G. Reinhard *et al.*, Z. Phys. A **323**, 13 (1986).

[6] A. Bouyssy *et al.*, Phys. Rev. C **36**, 380 (1987).

[7] B. ter Haar and R. Malfliet, Phys. Rep. **149**, 207 (1987).

[8] H. Müther, R. Machleidt, and R. Brockmann, Phys. Lett. B **202**, 483 (1988); Phys. Rev. C **42**, 1981 (1990).

[9] J. Boguta and J. Rafelski, Phys. Lett. **71B**, 22 (1977).

[10] F. E. Serr and J. D. Walecka, Phys. Lett. **79B**, 10 (1978).

[11] B. D. Serot and J. D. Walecka, Phys. Lett. **87B**, 172 (1979).

[12] P. Ring and P. Schuck, *The Nuclear Many-Body Problem* (Springer, Berlin, 1980).

[13] B. Grammaticos and A. Voros, Ann. Phys. (N.Y.) **123**, 359 (1979); **129**, 153 (1980).

[14] E. Wigner, Phys. Rev. **40**, 749 (1932).

[15] D. Von-Eiff and M. K. Weigel, Z. Phys. A **339**, 63 (1991).

[16] D. Von-Eiff, S. Haddad, and M. K. Weigel, Phys. Rev. C **46**, 230 (1992).

[17] M. K. Weigel, S. Haddad, and F. Weber, J. Phys. G **17**, 619 (1991).

[18] M. Centelles *et al.*, Nucl. Phys. **A519**, 73c (1990).

[19] C. Speicher, R. M. Dreizler, and E. Engel, Ann. Phys. (N.Y.) **213**, 312 (1992).

[20] H. Krivine, M. Casas, and J. Martorell, Ann. Phys. (N.Y.) **200**, 304 (1990).

[21] M. Centelles *et al.*, Nucl. Phys. **A537**, 486 (1992).

[22] M. Centelles *et al.*, University of Barcelona report, 1992.

[23] V. M. Strutinsky, Nucl. Phys. **A95**, 420 (1967); **A122**, 1 (1968).

[24] M. Centelles *et al.*, Nucl. Phys. **A510**, 397 (1990).

[25] Hsiao-bai Ai *et al.*, Phys. Rev. C **39**, 236 (1989).

[26] S. Marcos *et al.*, Phys. Rev. C **39**, 1134 (1989).

[27] M. Jetter, F. Weber, and M. K. Weigel, Europhys. Lett. **14**, 633 (1991).

[28] F. Weber and M. K. Weigel, Z. Phys. A **330**, 249 (1988).

[29] A. Bouyssy *et al.*, Phys. Rev. Lett. **55**, 1731 (1985).

[30] C. J. Horowitz and B. D. Serot, Nucl. Phys. **A464**, 613 (1987).

[31] F. Weber and M. K. Weigel, Nucl. Phys. **A493**, 549 (1989).

[32] J. Ramschütz (private communication).

[33] M. Brack, C. Guet, and H.-B. Håkansson, Phys. Rep. **123**, 275 (1985).

[34] H. de Vries, C. W. de Jager, and C. de Vries, At. Data Nucl. Data Tables **36**, 495 (1987).

[35] P. X. Ho *et al.*, Nucl. Phys. **A179**, 529 (1972).

[36] J. Heisenberg *et al.*, Phys. Rev. Lett. **23**, 1402 (1969).

[37] W. D. Myers and W. J. Swiatecki, Ann. Phys. (N.Y.) **55**, 395 (1969).

[38] M. Durand, P. Schuck, and X. Viñas, Institut des Sciences Nucléaires de Grenoble report, 1991.

[39] W. J. Swiatecki, Nucl. Phys. **A542**, 195 (1992).

[40] W. A. Barker and Z. V. Chraplyvy, Phys. Rev. **89**, 446 (1953).

[41] J. M. Eisenberg and W. Greiner, in *Nuclear Models, Nuclear Theory* (North-Holland, Amsterdam, 1975), Vol. 1, p. 196.